CONF-781202--31

CYCLIC STRESS-STRAIN BEHAVIOR OF ERNiCr-3 WELD FILLER METAL*

V. B. Baylor, M. K. Booker, J. P. Strizak, and R. L. Klueh
Metals and Ceramics Division
Oak Ridge National Laboratory
Oak Ridge, Tennessee 37830

ABSTRACT

Analytical representations were developed for the fatigue life and cyclic stress-strain response of AWS A5.14 Class ERNiCr-3 as observed during strain controlled cycling at a strain rate of 4×10^{-3}/s over strain ranges from 0.35 to 3.0% at 25, 343, 538 and 593°C. Specific areas studied include fatigue life as a function of strain, cyclic hardening and softening during testing, development of cyclic stress-strain curves from stress-strain amplitude coordinates, and development of bilinear representations of cyclic stress-strain behavior as suggested by current advanced design techniques.

At elevated temperatures, the fatigue life of ERNiCr-3 is reduced and the material cyclically hardens. At room temperature, some hardening due to cycling is displayed initially, followed by softening early in the test. The bilinear constants, E_m and C, are independent of temperature and strain rate, however, K_i is not. The power law, $\Delta\sigma = A(\Delta\varepsilon_p)^n$, adequately describes the cyclic stress-strain behavior at low strains. By bilinearization, the power law can be extended to predict K_i.

---

*Research sponsored by the Reactor Research and Technology Division, U.S. Department of Energy under contract W-7405-eng-26 with the Union Carbide Corporation.

DISCLAIMER

INTRODUCTION

Nickel-chromium filler metals have high strength and tolerate dilution by many metals without reduction in mechanical properties and without becoming crack sensitive at elevated temperatures.[1,2] They are the most widely used materials for producing high quality welds between dissimilar metals,[1,2] such as austenitic and ferritic steels, especially for use at high temperatures where unequal thermal expansion coefficients can cause relatively high thermal stresses, especially at the interface between ferritic steel and weld metal.[3] Nickel base weld metals are more suitable than iron base weld metals since they have an intermediate coefficient of thermal expansion between those of commonly used austenitic and ferritic steels, nearer to that of the ferritic.[1,2] Therefore, the highest stresses on the joint as a result of unequal expansion occur in the stronger, austenitic steel side.[1,2,4]

Present plans require that the steam generator system for the Liquid-Metal Fast Breeder Reactor (LMFBR) be constructed mainly of annealed ferritic 2 1/4 Cr-1 Mo steel.[6] Piping in this system may be subjected to temperatures as high as 517°C.[4,5] Since other components within the piping system are austenitic, transition joint weldments will be needed as connectors. A schematic cross section of the proposed transition joint is shown in Fig. 1.

Specifically, 2 1/4 Cr-1 Mo is welded to alloy 800H with AWS A5.14 Class ERNiCr-3 [67 Ni-18 to 22 Cr-2.5 to 3.5 Mn-2.0 to 3.0 (Nb+Ta)-3.0 Fe-0.10 C, wt %], commonly known as Inconel 82, using the hot wire automatic gas tungsten-arc process. ERNiCr-3 is a conventional nickel-chromium filler metal often used in austenitic/ferritic dissimilar metal joints. It is also used

for joining alloy 800H to itself.[1,2] Alloy 800H is used as a spool piece to grade the transition of thermal expansion coefficients across the weldment, and thus to lower projected thermal stresses.[3] The alloy 800H is welded to type 316 stainless steel using a filler of 16-8-2 (16 Cr-8 Ni-2 Mo-bal Fe, wt %) stainless steel. Further information regarding this joint design can be found elsewhere.[3,4]

Transition joints have been successfully used in commercial fossil-fired power plants for many years with some failures in the ferritic material adjacent to the fusion zone. In nuclear systems, the consequences of failure are particularly serious, and a design lifetime of 30 years is typically desired for joints. Mechanical properties data for weld metals are not currently required for design in Section VIII and Section III of the ASME Boiler and Pressure Vessel Code of Code Case 1592. The mechanical behavior of the weld metal, however, may affect the magnitude of the stress levels in the heat-affected zone (HAZ) in the 2 1/4 Cr-1 Mo steel, which is considered to be the critical region for failure.[3,5,7] As a result, advanced design techniques[8,9] for the LMFBR are beginning to consider the mechanical properties of weld metals, so that the characteristics of all involved structural materials can be incorporated in the joint design.

Tensile data for ERNiCr-3 have been recently acquired [10,11,12,13] and the elastic constants have been determined.[14] Analysis of available creep and creep-rupture data has been performed.[11,12,15,16] Because weldments of this type will be exposed to extensive cyclic loading,[4] the elevated temperature fatigue properties of ERNiCr-3 are being investigated.[17,18]

The purpose of this study was to suggest analytical representations for the cyclic stress-strain response of ERNiCr-3 as observed during strain controlled continuous cycling fatigue tests. Areas to be discussed include: number of cycles to failure as a function of plastic and total strain, cyclic hardening and softening during testing, development of cyclic stress-strain curves from hysteresis loop tips from similar tests at different constant strain ranges, and development of predictions of cyclic behavior based on bilinear approximations of monotonic and cyclic stress-strain behavior. The bilinear representation is an inelastic analysis simplification which was originally suggested for austenitic steels[8] but was extended here to provide a framework within which to analyze the behavior of ERNiCr-3.

Generally, the fatigue behavior of a weldment is greatly affected by factors such as the presence or absence of defects,[19] the joint geometry,[19] and the fatigue behavior of the individual materials over the temperature range and strain rate of interest. The anisotropy and heterogeneity of the weld metal are contributory factors which are recognized but not considered in this study. The scope of this analysis was limited to two types of welds and two specimen orientations. Thus, the findings are preliminary in nature.

EXPERIMENTAL PROCEDURE

Material

Annealed 2 1/4 Cr-1 Mo steel plates (ASME SA-387, Grade D), 19-mm-thick, were welded using the automatic gas tungsten arc (GTA) process with either hot- or cold-wire ERNiCr-3 weld filler metal additions. The GTA process

using hot-wire filler additions produces high quality welds since dilution is minimized and a higher deposition rate is allowed per pass. Typically, 40 weld pases were required for cold-wire and 16—18 weld passes were required for hot-wire joints. A typical vendor analysis of ERNiCr-3 wire is given below:

Chemical Composition, wt %

Cr	Fe	Mn	Nb	Ti	Ni
18.0	1.8	3.0	2.3	0.3	bal

The joint geometry of the weldments was a 30°-included-angle V-groove with a 32 mm root opening and a backing strip. The nominal welding parameters were as follows: 150A and 10V, with a travel speed of about 0.9 mm/s using cold-wire filler additions; and 400A and 15V torch current, with a travel speed of about 0.25 mm/s, with hot-wire heated by 110A and fed at about 12.7 mm/s. The joints were radiographed as were the specimens; those specimens free of defects were post-weld heat-treated in air at 732°C for 1 hr.

For the weld made with cold-wire filler additions, the chemical composition of the stress-relieved weld metal was determined for three positions of the weld cross section: the center of the cross section, the edge near the 2 1/4 Cr-1 Mo steel, and midway between these two regions as shown in Fig. 2. Some dilution was apparent as increased iron concentration was found in weld metal areas adjacent to the fusion line. No other elements showed evidence of dilution. An iron concentration profile was determined by probing the upper half of the cross section of the specimen with a static spot x-ray step scan every 1.25 mm (Fig. 3).

The hardness and microstructures of a typical weldment made with cold-wire filler additions are shown in Fig. 4. The hardness profile shows the ERNiCr-3 deposit to be harder than the annealed 2 1/4 Cr-1 Mo steel. The microstructure of the weldment is complicated, reflecting factors such as the difference in composition between ERNiCr-3 and 2 1/4 Cr-1 Mo and their varying response to heat treatment. A typical weld metal or cast microstructure can be observed in etched ERNiCr-3 weld metal (Figs. 5–6).

Fatigue and tensile specimens were machined from the central portion of the weld such that the uniform gage lengths were completely weld metal. Fatigue specimens (6.35-mm diam by 16-mm long uniform gage) were prepared in either longitudinal or transverse orientations. The buttonhead type tensile specimens (3.18-mm diam by 28.6-mm gage length) were all oriented longitudinally (major axis parallel to the line of fusion). All fatigue specimens were buffed longitudinally so that circumferential grinding marks were removed, leaving a 0.20–0.28 μm surface finish. Specimens were subsequently radiographed again prior to testing. Additional information on the specimens used can be found elsewhere.[13,17,20]

Testing Procedure

Monotonic stress-strain tests were made on an Instron machine with crosshead speeds of 8.5 and 0.085 μm/s. Forty-three tests (34 cold-wire and 9 hot-wire) were conducted at a nominal strain rate of 3×10^{-4}/s and eight cold-wire tests were conducted at 3×10^{-6}/s nominally, over the temperature range 25–732°C. Nineteen fatigue test specimens made with cold-wire filler additions and twenty-nine hot-wire specimens were tested over the temperature range 25–593°C. All of the fatigue tests were conducted in axial strain

control using strain ranges from 0.35—3.0% at a nominal strain rate of 4×10^{-3}/s. Three longitudinal specimens were tested at 343°C; all other fatigue specimens had transverse orientations. An axial extensometer was used, and heat was provided by an induction coil with an air environment. Additional information on test procedure is available.[11,12,13,17]

RESULTS

Fatigue Life

The first quarter-cycle of a fatigue test produces a curve similar to the tensile loading curve, usually showing a yield point and regions of elastic and plastic flow. A complete cycle consists of tensile loading followed by unloading, compression and unloading, resulting in a hysteresis curve (Fig. 7). The abscissa represents total strain; the total strain range, $\Delta\varepsilon_t$, can be measured as the horizontal distance between the tips of the loop. The total stress is the ordinate; the stress range, $\Delta\sigma$, is indicated by the vertical distance between the loop tips.

Cyclic life (N_f) was defined to be the number of cycles to specimen failure (separation into two halves). The total strain range as a function of the number of cycles to failure is shown in Fig. 8. A temperature dependence was noted; specimens tested at 593°C failed earlier than those at lower temperatures. In addition, the fatigue life of material made by the hot-wire GTA process was slightly superior to that of cold-wire material. The strain controlled low cycle fatigue behavior of as-deposited and stress-relieved ERNiCr-3 weld metal is more fully described elsewhere.[17]

The plastic strain range (total inelastic strain range) was also related to cycles to failure (Fig. 9). In a typical plot, often no temperature

dependence is seen,[21] but for ERNiCr-3, specimens tested at 593°C showed a reduced fatigue life compared with lower test temperatures. In addition, it can be seen again that the hot-wire material has a slightly better resistance to cyclic loading than does the cold-wire. Analytical predictions of fatigue life shown in Figs. 8-9 will be discussed below.

Cyclic Stress-Strain Behavior

Cyclic Hardening and Softening

Cyclic hardening or softening of a specimen during strain controlled loading is indicated by a change in the amount of applied stress, with number of cycles, that is required to maintain the imposed strain range.[22] For many materials, this phenomenon is manifested by rapid cyclic hardening, usually complete after a few cycles, followed by a period of stability.[22] ERNiCr-3 often displays this typical pattern. Figures 10—11 illustrate the detailed hardening and softening behavior during continuous cycling at 4×10^{-3}/s. At low strain ranges ($\leq$ 0.6%), rapid initial hardening was followed by stable stress levels at all temperatures. Maximum stress levels were reached at a lower fraction of total life for the room temperature tests; that is, hardening was more gradual at elevated temperatures.

This pattern of change was obtained for all low strain range tests; at higher strain ranges ($\geq$ 1.95%), the hardening behavior of ERNiCr-3 is more complicated. At room temperature with a 3% strain range, the test specimens exhibited rapid initial hardening followed by a slight softening. For a strain range of 1.95% at 343°C, a small amount of cyclic hardening took

place after the initial rapid hardening. At higher temperatures, 538 and 593°C, no sharp rapid hardening appeared as before. At these higher strain ranges, the specimens gradually hardened to reach a maximum stress value after three-fourths the fatigue life.

Just before fatigue failure, many materials exhibit a decrease in tensile stress amplitude, or apparent softening, which we hypothesize to be due to the formation of a crack. ERNiCr-3 displays this behavior, with softening occurring earlier in the cyclic life of the room-temperature test specimens than in those at elevated temperatures.

Cyclic Stress-Strain Curves

The cyclic hardening behavior of ERNiCr-3 is shown also by the cyclic stress-strain curves. The cyclic stress-strain curve measures the resistance of the material to deformation by cyclic loading. These curves can be directly compared with monotonic stress-strain curves. The cyclic curve may be quite different from the monotonic loading curve, showing the change in response due to cyclic loading. If the cyclic curve lies above the monotonic curve, then the material exhibits cyclic hardening, and if the cyclic curve is lower, the material cyclically softens.[22]

A hysteresis loop from a fatigue test is partially characterized by a strain range, $\Delta\varepsilon_t$, and a stress range, $\Delta\sigma$. When measured from the origin, the coordinates of the loop tip correspond to $\Delta\varepsilon_t/2$ (strain amplitude) and $\Delta\sigma/2$ (stress amplitude). A nest of hysteresis curves can then be represented by these coordinates from measured values of $\Delta\varepsilon_t$ and $\Delta\sigma$ as shown in Fig. 12.

Cyclic stress-strain curves were constructed from the locus formed by stress-strain amplitude coordinates at different strain ranges[22] at a given temperature using 10th cycle, 100th cycle, and half-life values of $\Delta\sigma$.

For ERNiCr-3, cyclic stress-strain curves lie above the monotonic curves at all temperatures indicating hardening due to cycling. In addition, at elevated temperatures at low strain, the 10th cycle curve is the lowest cyclic curve, with the 100th cycle curve being higher and the $N_f/2$ curve the highest. At room temperature, however, the $N_f/2$ curve lies below the 100th cycle curve, showing evidence of softening relatively early in the test. Analytical predictions of cyclic stress-strain behavior shown in Fig. 12 will be discussed below.

Bilinear Representations of Stress-Strain Behavior

Bilinear Approximation

Monotonic bilinear stress-strain curves (Fig. 13) were constructed for ERNiCr-3 as described in Ref. 18. These curves consist of a linear elastic portion with a slope equal to Young's modulus, E, and a linear "plastic" portion with a slope equal to E_m. The two lines intersect at a stress value of σ_y, or the bilinear yield strength. Two bilinear stress-strain constants, C and κ_0, are calculated as follows:

$$C = \frac{2}{3}\left(\frac{E \times E_m}{E - E_m}\right) ,$$

and

$$\kappa_0 = \frac{\sigma_y^2}{3} ,$$

where

κ_0 is a measure of the size of the loading, or yield surface, and

C is the slope of the deviatoric stress-plastic strain line.

Figure 14 shows how the plastic portion of the bilinear curve is constructed. The plastic line passes through the points on the stress-strain curve where the stress corresponds to the strain, ε_{max} and $\varepsilon_{max}/2$. A second bilinearization method recommended for ferritic materials[9] was considered, but was rejected for this application as described in Ref. 18.

For cyclic stress-strain curves, values for E_m, and consequently C, are assumed to be the same as those for the corresponding monotonic tests at a particular strain. Figure 7 shows how the curve is constructed. Lines of slope E_m are placed on the upper and lower portions of the hysteresis loop such that the two shaded areas in the figure are equal. The vertical distance between the upper line and the point where the lower line intersects the vertical is denoted by 2σ. The bilinear constant, κ_i, is then calculated from

$$\kappa_i = (2\sigma)^2/12 \ , \qquad (1)$$

where

κ_1 is calculated from 2σ at the 10th cycle,

κ_2 is calculated from 2σ at the 100th cycle, and

κ_3 is calculated from 2σ at a cycle near the fatigue half-life, or $N_f/2$.

The procedure for determining E_m, C, and κ_i values can be found in Ref. 8.

Bilinear Monotonic Stress-Strain Behavior

The bilinear constants E_m, C, and κ_0 were calculated for various values of ε_{max} at four test temperatures, 25, 316, 566, and 621°C, and the two different strain rates. These temperatures were the closest to the test temperatures used for the cyclic stress-strain tests. We found E_m to be independent of temperature and strain rate as shown in Fig. 15. There was also no significant difference observed between behavior of the hot- and cold-wire deposited material. A single mean curve was drawn through the data to produce the values used for cyclic analysis.

The slope C is a function of E_m and E. Even though E varies somewhat with temperature, this dependency does not significantly affect the value of C. Since E_m is relatively independent of temperature then C is relatively independent of temperature also.

Whereas both E_m and C are independent of temperature and strain rate, κ_0 is not. There was no real difference between the hot- and cold-wire data, but κ_0 varied sometimes with strain rate. At 316°C, no discernible effects of strain rate were observed; however, at 566°C strain rate had a significant bearing on κ_0. This diversity is verified by Ref. 13 where significant differences in yield strengths at the two strain rates were noted at temperatures above 450°C. Figure 16 shows κ_0 as a function of temperature at a typical strain range. There is a general, but not necessarily monotonic, trend for κ_0 to decrease with temperature.

Bilinear Cyclic Stress-Strain Behavior

Values of κ_i were computed from the 10th cycle, 100th cycle, and $N_f/2$ cycle hysteresis loops. These fatigue test data were not generated for the express purpose of bilinear analysis; thus, in cases where the specific loop was not available, the closest number loop was used. κ_i as a function of strain amplitude is shown in Figs. 17–19.

For many materials, $\kappa_3 > \kappa_2 > \kappa_1 > \kappa_0$, indicating cyclic hardening. ERNiCr-3 displays this hardening behavior at elevated temperatures. At room temperature, however κ_3 is lower than κ_2, thus indicating cyclic softening. At the 10th cycle, room-temperature specimens hardened more than elevated temperature specimens, but by $N_f/2$ the room-temperature ERNiCr-3 became softer than the elevated temperature test material at a strain rate of 4×10^{-3}/s. There is no indication, however, that the material will soften to the extent that κ_3 values would approach the monotonic level (κ_0). The room-temperature cyclic stress-strain behavior of ERNiCr-3 is complex, and not enough data are available to yield a full understanding of this behavior.

Regression Analysis

Prediction of Cyclic Stress-Strain Behavior

The relationship between cyclic stress and plastic strain can be expressed by a power function similar to that for the monotonic curve, or described by a linear expression on log-log coordinates. The slope of the line is the cyclic strain hardening exponent. Cyclic stress-strain curves are adequately represented by[22]

$$\Delta\sigma/2 = t(\Delta\varepsilon_p/2)^u \ , \tag{2}$$

or, equivalently,

$$\Delta\sigma = A(\Delta\varepsilon_p)^n \ . \tag{3}$$

where

$\Delta\sigma/2$ = cyclic stress amplitude,

A = cyclic strength coefficient,

$\Delta\varepsilon_p/2$ = cyclic plastic strain amplitude, and

n = cyclic strain hardening exponent.

Values for A and n as determined for the present data by least-squares analysis are listed in Table 1.

Table 1. Cyclic hardening constants for cyclic stress-strain curves, strain controlled fatigue tests at 4×10^{-3}/s strain rate.

Temperature (C)	$\Delta\sigma = A(\Delta\varepsilon_p)^n$					
	10th cycle		100th cycle		$N_f/2$ cycle	
	A	n	A	n	A	n
22	885	0.118	1030	0.141	1020	0.106
343	730	0.190	895	0.262	1040	0.117
538	740	0.148	940	0.221	1040	0.148
593	670	0.169	920	0.283	985	0.170

The following was used to define the plastic strain amplitude for the 10th, 100th, and $N_f/2$ cycles:

$$\frac{\Delta\varepsilon_p}{2} = \frac{\Delta\varepsilon_t}{2} - \frac{\Delta\sigma}{2E}, \tag{4}$$

where

$\Delta\varepsilon_t$ = total strain range,

$\Delta\sigma$ = stress range at indicated cycle, and

E = Young's modulus.

Young's modulus values used for predicting cyclic stress-strain behavior were averaged from several hysteresis loops at a given temperature.[17] By combining Eqs. (2) and (4), data from the loops can be fit by an equation of the form:

$$\frac{\Delta\varepsilon_t}{2} = \frac{\Delta\sigma}{2E} + \frac{(\Delta\sigma/A)^{1/n}}{2} \quad . \tag{5}$$

Since ε_{max} is equivalent to $\Delta\varepsilon_t/2$, Fig. 12 illustrates fits of Eq. (5) for 538°C as $\Delta\sigma/2$ is plotted against ε_{max}. No discernible differences were noted between results from hot- and cold-wire tests or between transverse and longitudinally oriented specimens.

As shown in Figs. 20–22, $\Delta\sigma$ was plotted against 2σ. In general, a direct proportionality was observed, namely $2\sigma = 0.83\ \Delta\sigma$, for all cases except room temperature tests. Using this value and substituting ε_{max} for $\Delta\varepsilon_t/2$, Eq. (5) becomes:

$$\varepsilon_{max} = \frac{1.2(2\sigma)}{2E} + 1/2\left[\frac{1.2(2\sigma)}{A}\right]^{1/n} . \qquad (6)$$

Since $\kappa_i = (2\sigma)^2/12$, then

$$\varepsilon_{max} = \frac{1.2\sqrt{12\kappa_i}}{2E} + 1/2\left[\frac{1.2\sqrt{12\kappa_i}}{A}\right]^{1/n} . \qquad (7)$$

Predicted κ_i curves based on Eq. (7) for elevated temperature tests are shown in Figs. 17–19. For the room temperature tests, a best-fit line was drawn so that $2\sigma = b\Delta\sigma^a$. Values for a and b are listed in Table 2. A similar equation to Eq. (7) was derived for room temperature κ_i values; the actual data and predictions are also shown in Figs. 17–19.

Table 2. Best fit values for 2σ as a function of $\Delta\sigma$ for cyclic stress-strain tests at room temperature, strain rate of 4×10^{-3}/s

Cycle	Constants of $2\sigma = b\Delta\sigma^a$	
	a	b
10th	1.0	0.83
100th	1.165	0.244
$N_f/2$	1.606	0.012

Figure 17 shows κ_1 curves at the four temperatures. As would be expected, the curve for 25°C is the highest and the curve for 593°C is the lowest. The 343 and 538°C values do not differ much and fall between the other two curves.

For ε_{max} <0.75%, the 343°C curve is slightly lower than that for 538°C. At the 100th cycle (Fig. 18), all the curves are grouped together to some extent, but the curve for 343°C has dropped relative to the others to become the lowest. At $N_f/2$ (Fig. 19), the relative κ_3 values show another change. The curve for 25°C is the lowest and is almost identical to the 593°C curve. The 538 and 343°C curves are also similar, but the 538°C curve is slightly higher. The relative curve positions are the same in Figs. 17 and 19, except that in Fig. 17 the room-temperature curve is the highest and becomes the lowest by $N_f/2$ (Fig. 19).

Fatigue Life Prediction

A common method for description of fatigue life in cycles (N_f) as a function of total strain range ($\Delta\varepsilon_t$) involves the use of power-law relationships between N_f and the elastic ($\Delta\varepsilon_e$) and plastic ($\Delta\varepsilon_p$) strain ranges. Thus,

$$\Delta\varepsilon_e = AN_f^{-\alpha} , \tag{8}$$

and

$$\Delta\varepsilon_p = BN_f^{-\beta} , \tag{9}$$

so that

$$\Delta\varepsilon_t = \Delta\varepsilon_e + \Delta\varepsilon_p = AN_f^{-\alpha} + BN_f^{-\beta} . \tag{10}$$

For the current data, we found $\alpha = 0.688$, $A = 113.9$, $\beta = 0.102$, and $B = 1.32$ from room temperature to 538°C. At 593°C we found $\alpha = 0.664$, $A = 51.46$, $\beta = 0.108$, and $B = 1.24$. Figure 9 compares available data with

predictions from Eq. (8), while Fig. 8 compares data with predictions from Eq. (10). The equations were developed from data for hot-wire material only. The data for cold-wire material in the figures are shown for comparison only.

It should be noted that $\Delta\varepsilon_e$ is defined by $\Delta\sigma/E$, where $\Delta\sigma$ is the total stress range and E is Young's modulus. Making this substitution, solving Eqs. (8) and (9) for N_f, and noting that N_f must equal itself yields

$$\left(\frac{\Delta\sigma/E}{A}\right)^{-1/\alpha} = \left(\frac{\Delta\varepsilon_p}{B}\right)^{-1/\beta} \tag{11}$$

Equation (11) is of the same form as Eq. (3). Thus, the application of the commonly used power-law fatigue life equations constitutes an implicit assumption that the power-law cyclic stress-strain equation is also valid.

DISCUSSION

The behavior of weldments in detail is the subject of continuing studies directed toward understanding how the abrupt change in thermal and mechanical properties across a transition joint affects the service life of the joint. Although consideration of the cyclic stress-strain behavior of the weld metal is not specifically mandated by current codes, advanced numerical finite element analyses of elastic-plastic stress-strain states require complete knowledge of the mechanical properties of all involved materials.[8] The current analysis was performed to provide relevant data for these design techniques.

The effect of any material in a joint, particularly the weld metal, on the behavior of the entire weldment is a complex subject requiring further investigation. For example, it has been shown that the thermal stresses of one possible transition joint have been reduced by the use of ERNiCr-3 with alloy 800H as a spool piece, placing the highest calculated stresses on the alloy 800H side of the joint.[4] Previous studies[13,15,16] have indicated that ERNiCr-3 is comparable in strength to alloy 800H,[23] but is significantly stronger than the 2 1/4 Cr-1 Mo steel[24,25] to which it will be welded. It is unclear how much the difference in strength between materials will affect the behavior of the critical region of the HAZ in the 2 1/4 Cr-1 Mo steel.

Only a limited amount of data is currently available. Most analyses treat various regions of the weldment as homogeneous and isotropic, whereas in reality, an accurate description would include continually varying mechanical properties with respect to location in the weld. Even so, current design techniques have become relatively sophisticated in their consideration of properties such as fatigue and creep. More data are needed to fully characterize the cyclic stress-strain response of ERNiCr-3 at temperatures and strain rates not yet investigated. In addition, detailed further study and modeling are necessary to determine how this cyclic stress-strain response of the weld metal affects the behavior of the entire transition joint.

SUMMARY

The following conclusions were drawn regarding the cyclic stress-strain behavior of ERNiCr-3:

1. ERNiCr-3 responds to cyclic loading by increasing resistance to deformation, or cyclic hardening. At low strain ranges, the material exhibits rapid initial hardening followed by a nearly steady-state condition, until apparent softening occurs just before failure. At high strain ranges at elevated temperatures, the hardening is much more gradual; the maximum stress is not reached until at least three-fourths of the fatigue life. ERNiCr-3 displays some cyclic softening at room temperature.

2. Comparison of cyclic and monotonic stress-strain data was accomplished through the construction of cyclic stress-strain curves from the stress and strain amplitude coordinates. It was found that the isothermal power law, Eq. (2), adequately describes the response of ERNiCr-3 to cyclic loading up to $\varepsilon_{max} = 1.0\%$. At higher strains, the cyclic stress-strain behavior of this material is complex and requires further investigation.

3. Although the fatigue life of ERNiCr-3 filler metal made by the automatic gas tungsten-arc process with hot-wire filler additions is slightly superior to that made with cold-wire additions, neither the monotonic nor cyclic bilinear stress-strain constants were significantly dependent on how the weld filler metal was added. It appears that the two bilinear slopes, E_m and C, are independent of strain rate and temperature for strains $\leq 2\%$. Thus, the slope of the upper and lower lines for the bilinear approximation of the hysteresis loop is determined by the strain range

only. In addition, the cyclic stress-strain response of ERNiCr-3 did not appear to vary due to the orientation of the specimen with regard to the line of fusion, that is, transverse versus longitudinal.

4. Values for κ were determined for the monotonic tests (κ_0) and at three cycles of the fatigue tests, 10th (κ_1), 100th (κ_2), and $N_f/2$ (κ_3). Although monotonic and cyclic tests were generally not conducted at the same temperatures, by interpolation of monotonic data, we generally found that κ_1 was greater than κ_0. At elevated temperatures, κ increases isothermally with the number of cycles; at room temperature, κ decreases after the 100th cycle. Reasons for this somewhat complicated temperature dependence in the cyclic hardening behavior are not understood at this time.

5. For $\Delta\sigma$ values between about 450 and 1030 MPa, the equation $2\sigma = 0.83\ \Delta\sigma$ applies, but from the present data it is uncertain whether this relationship is valid for $\Delta\sigma$ values outside this range (or at other temperatures). The direct proportionality between $\Delta\sigma$ and 2σ observed for this material facilitates behavior analysis through an extension of the isothermal power law. One can directly determine κ from the stress range at a 4×10^{-3}/s strain rate at elevated temperatures. Data for $\Delta\sigma$ are generally more readily available than 2σ data since the stress range is frequently reported in fatigue tests. Also, $\Delta\sigma$ can be measured easier than 2σ, thus decreasing the analysis time.

6. The extensive scatter in the data causes a large uncertainty in the prediction of κ for strain rates and temperatures other than those for which data are available. At the present time, the strain rate and

temperature dependence of κ are complicated and not fully understood. This same complexity is observed in the temperature dependence of the monotonic tensile properties. More data are needed so that these relationships can be more adequately represented analytically.

REFERENCES

1. H. R. Conaway, "Part 5: Welding the Nickel Alloys; Dissimilar Metals, High-Temperature Service," *Welding Design and Fabrication,* June, 1977.

2. *Joining Huntington Alloys,* International Nickel Company, Inc., 1972.

3. J. F. King, G. M. Slaughter, and M. D. Sullivan, "Transition Joint Welding Development for LMFBR Steam Generator Design," pp. 82—1—5 in *Proceedings of the International Conference on Ferritic Steels for Fast Reactor Steam Generators,* British Nuclear Energy Society, London, 1977.

4. A. W. Dalcher and T. M. Yang, "High Temperature Elastic Analysis of Dissimilar Metal Welded Pipe Joints, pp. 1978—83 in *Proceedings of the Second International Conference on Mechanical Behavior of Materials,* American Society for Metals, August 1976.

5. J. F. King, *Behavior and Properties of Welded Transition Joints Between Austenitic Steels and Ferritic Steels — A Literature Review,* ORNL-TM-5193 (November 1975).

6. C. R. Brinkman, R. K. Williams, R. L. Klueh, and T. L. Hebble, "Mechanical and Physical Properties of 2 1/4 Cr-1 Mo Steel in Support of Clinch River Breeder Reactor Plant Steam Generator Design," *Nucl. Technol.* 28(3): 490—505 (1976).

7. C. R. Brinkman et al., "Mechanical Properties of Transition Joint Materials in Support of LMFBR Steam Generator Design," pp. 82—1—5 in *Proceedings of the International Conference on Ferritic Steels for Fast Reactor Steam Generators*, British Nuclear Energy Society, London, 1977.

8. C. E. Pugh, K. C. Liu, J. M. Corum, and W. L. Greenstreet, *Currently Recommended Constitutive Equations for Inelastic Analysis of FFTF Components,* ORNL-TM-3602 (September 1972).

9. C. E. Pugh et al., *Background Information for Interim Methods of Inelastic Analysis for High-Temperature Reactor Components of 2 1/4 Cr-1 Mo Steel,* ORNL-TM-5226 (May 1976).

10. *Incoloy Nickel-Iron-Chromium Alloys,* International Nickel Company, Inc. 1973.

11. R. L. Klueh and J. F. King, "Creep and Tensile Properties of Transition Weld Joint Materials," *Mechanical Properties Test Data for Structural Materials Quart. Prog. Rep. Jan. 31, 1977,* ORNL-5237, pp. 197—204.

12. R. L. Klueh and J. F. King, "Creep and Tensile Properties of Transition Weld Joint Materials, *Mechanical Properties Test Data for Structural Materials Quart. Prog. Rep. Apr. 30, 1977,* ORNL-5986, pp. 264—86.

13. R. L. Klueh and J. F. King, *Elevated-Temperature Tensile Properties of ERNiCr-3 Weld Metal*, ORNL-5354, (December 1977).

14. J. P. Hammond, "Elastic Constants in Weldment Structures," *Mechanical Properties Test Data for Structural Materials Quart. Prog. Rep. Jan. 31, 1976*, ORNL-5112, pp. 133–41.

15. R. L. Klueh and J. F. King, "Creep and Creep-Rupture Behavior of ERNiCr-3 Weld Metal," report in preparation.

16. M. K. Booker and R. L. Klueh, "An Interim Analytical Description of the Creep and Creep-Rupture Behavior of ERNiCr-3 Weld Metal," report in preparation.

17. C. R. Brinkman, J. P. Strizak, and J. F. King, "Elevated Temperature Fatigue Characterization of Transition Joint Weld Metal and Composite Material in Support of LMFBR Steam Generator Development," to be published.

18. V. B. Baylor, M. K. Booker, J. P. Strizak, and R. L. Klueh, *Stress-Strain Behavior of ERNiCr-3 Weld Filler Metal Under Strain Controlled Cyclic Loading*, ORNL-TM-6128 (January 1978).

19. H. Thielsch, *Defects and Failures in Pressure Vessels and Piping*, Reinhold Publishing Corp., New York, 1965.

20. C. R. Brinkman et al., *Interim Report on the Continuous Cycling Elevated Temperature Fatigue and Subcritical Crack Growth Behavior of 2 1/4 Cr-1 Mo Steel*, ORNL-TM-4993 (December 1975).

21. G. R. Halford, M. H. Hirschberg and S. S. Manson, *Temperature Effects on the Strainrange Partitioning Approach for Creep-Fatigue Analysis*, NASA TM X-68023.

22. J. Morrow, "Cyclic Plastic Strain Energy and Fatigue of Metals," pp. 45–87 in *Internal Friction, Damping, and Cyclic Plasticity, Stand. Tech. Publ.* 378, American Society for Testing and Materials, Philadelphia, 1965.

23. M. K. Booker, V. B. Baylor, and B. L. P. Booker, *Survey of Available Creep and Tensile Data for Alloy 800H*, ORNL-TM-6029 (January 1978).

24. M. K. Booker, T. L. Hebble, D. O. Hobson, and C. R. Brinkman, "Mechanical Property Correlations for 2 1/4 Cr-1 Mo Steel in Support of Nuclear Reactor Systems Design," *International Journal of Pressure Vessels and Piping*, Vol. 5, pp. 181-205, 1977.

25. M. K, Booker, "Analytical Description of the Effects of Melting Practice and Heat Treatment on the Creep Properties of 2 1/4 Cr-1 Mo Steel," *Effects of Melting and Processing Variables on the Mechanical Properties of Steel*, MPC-6, G. V. Smith, ed., The American Society of Mechanical Engineers, New York, 1977, pp. 323-343.

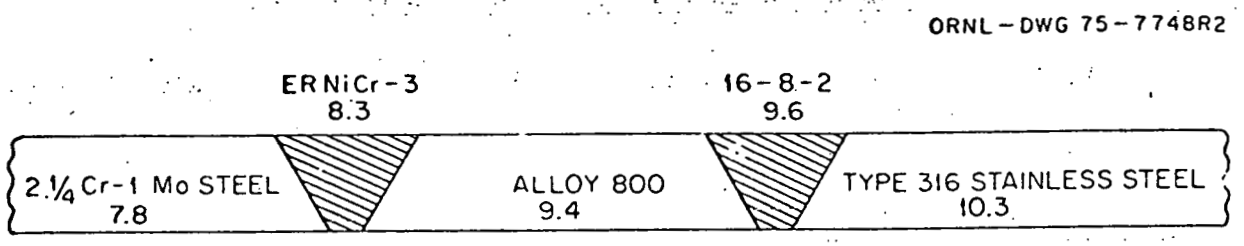

Fig. 1. Transition Joint Configuration. Mean coefficients of expansion from 22 to 538°C are noted below each material.[3]

ORNL-DWG 78-10228

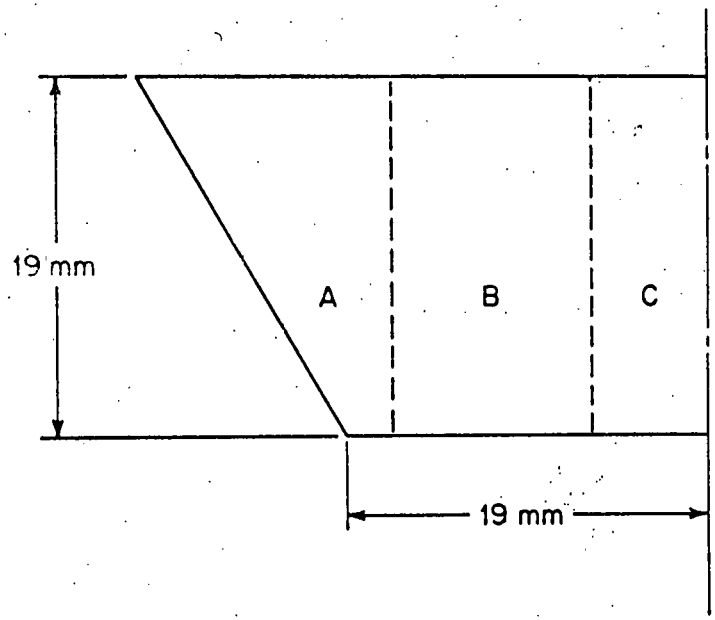

SPECIMEN	CHEMICAL COMPOSITION, wt% Cr	Fe	Mn	Nb	Ti
A	18	4.1	2.9	2.8	0.3
B	17	1.9	3.0	2.4	0.3
C	18	1.7	2.9	2.2	0.3
SPECIFICATION					
min	18.0		2.5	2.0	
max	22.0	3.0	3.5	3.0	0.75

Balance is Ni

Fig. 2. Cross-Section and Chemical Composition of Various Portions of the Weld.

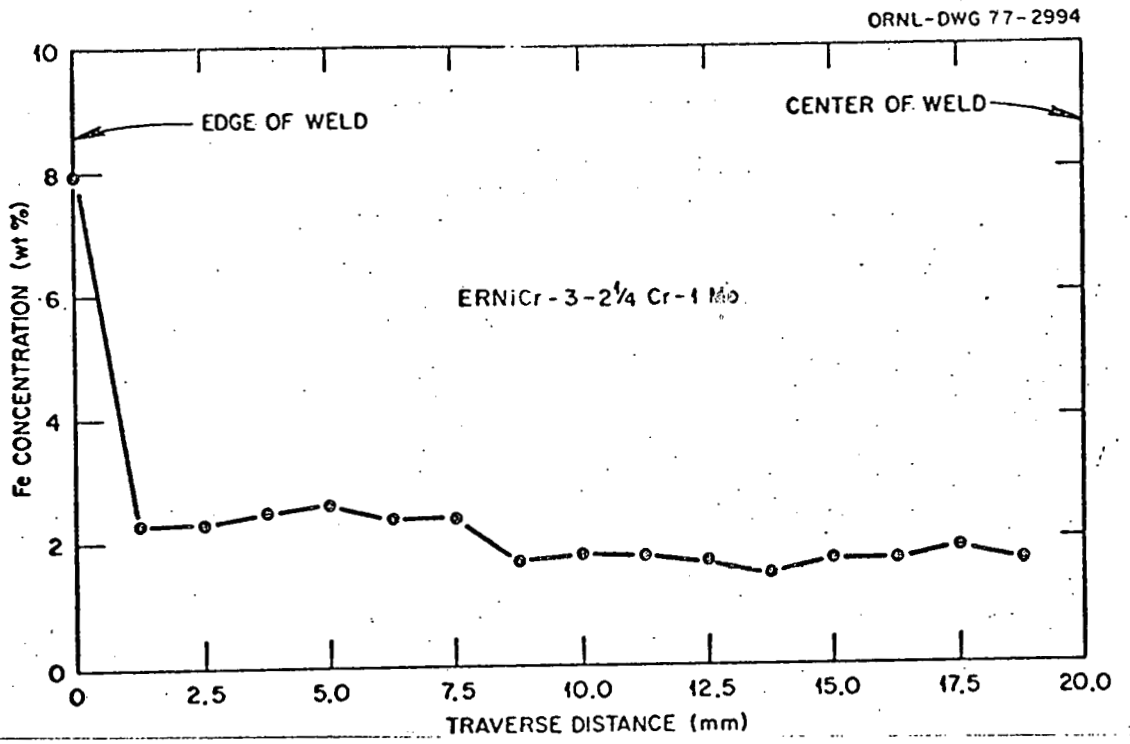

Fig. 3. Iron Concentration Profile of a Weld Made with Cold Wire Filler Additions.

PHOTO 2513-76

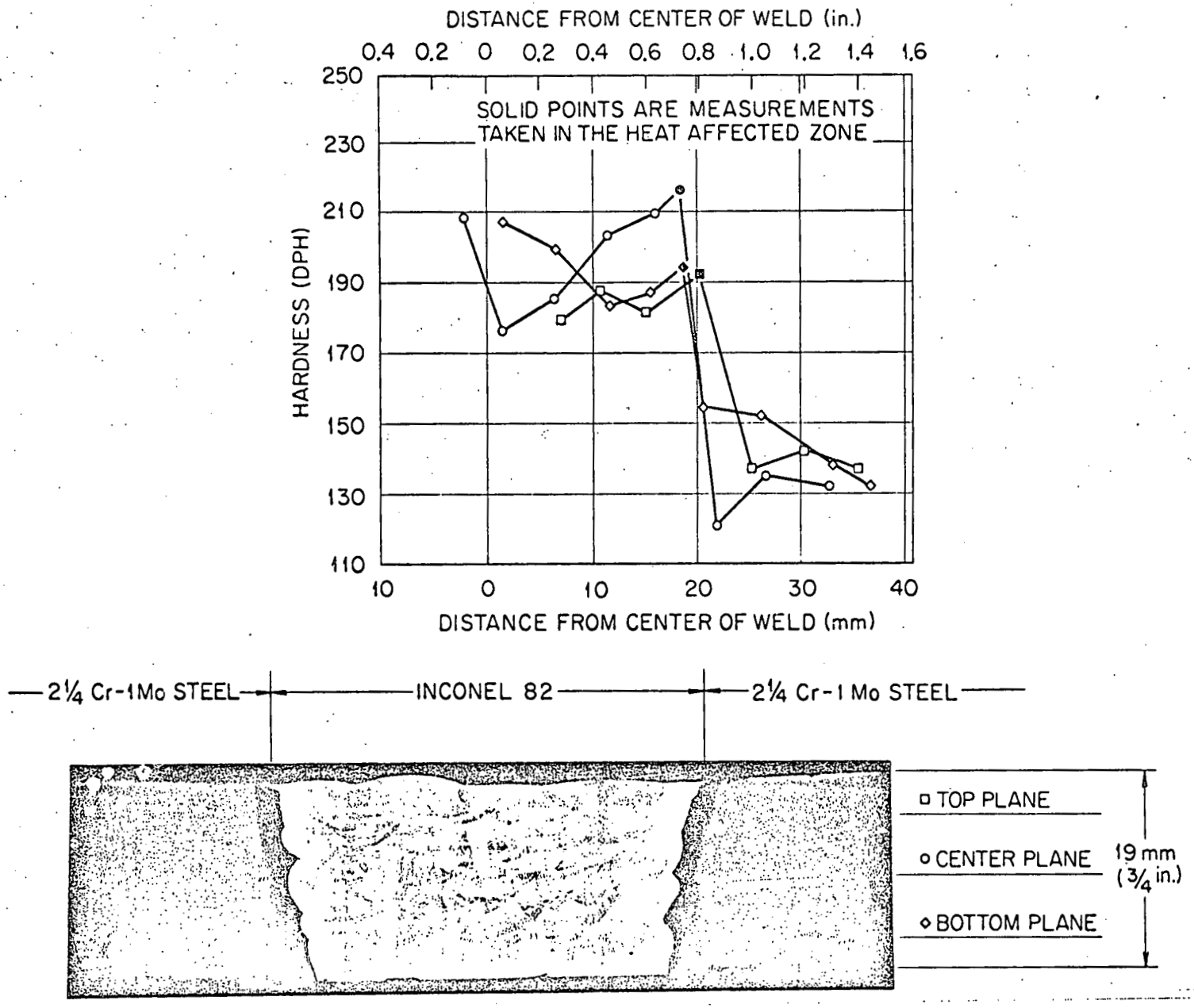

Fig. 4. Hardness Measurements on a Weldment Joining 2 1/4 Cr-1 Mo Steel with ERNiCr-3 Filler Metal. The weldment was fabricated by the automatic gas tungsten-arc process with cold wire filler additions and then stress relieved at 732°C for 1 hr.

ORNL-PHOTO 1156-77

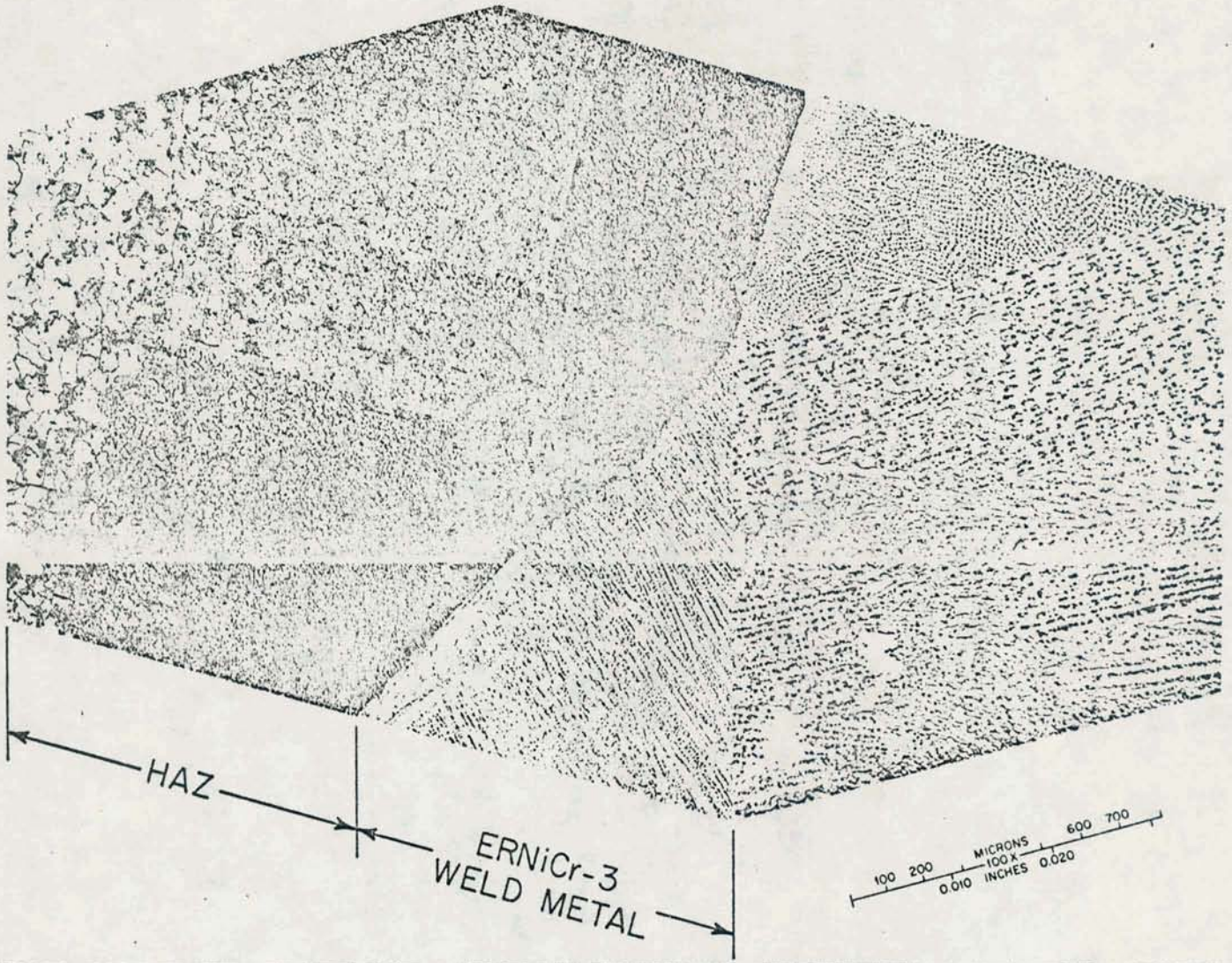

Fig. 5. Three Dimensional Photomicrograph Showing Microstructure Obtained by Welding 2 1/4 Cr-1 Mo Steel with ERNiCr-3. The weldment was prepared using the hot wire automatic gas tungsten-arc process.

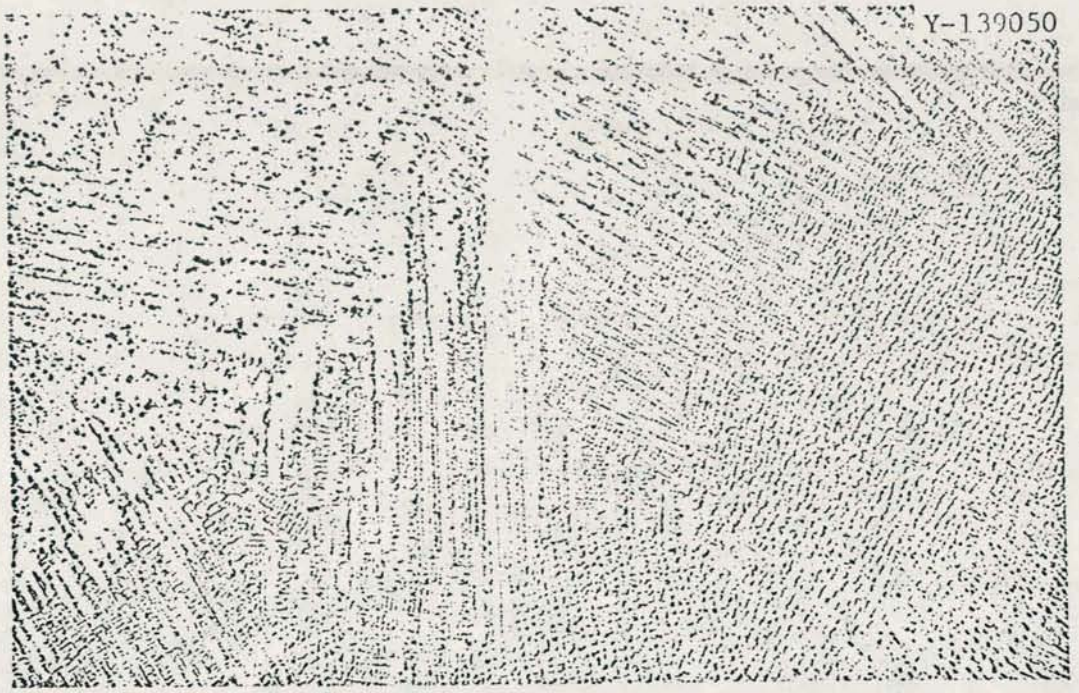

Fig. 6. Microstructure of Undeformed ERNiCr-3 Weld Metal Deposited by Cold Wire Automatic Gas Tungsten-Arc Process.

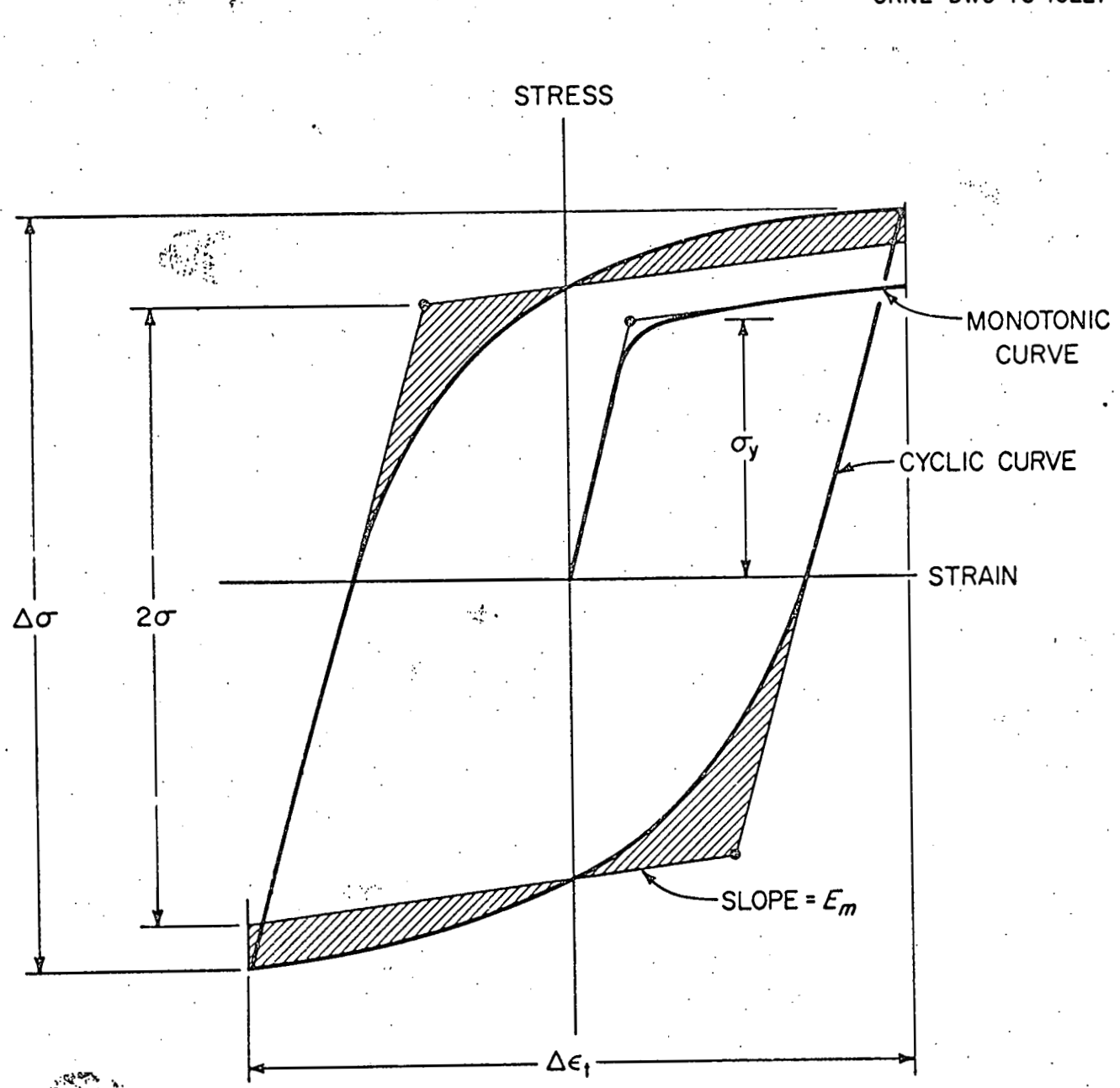

Fig. 7. Typical Hysteresis Curve Generated by a Cyclic Stress-Strain Test. Bilinearization of the curve is shown also.

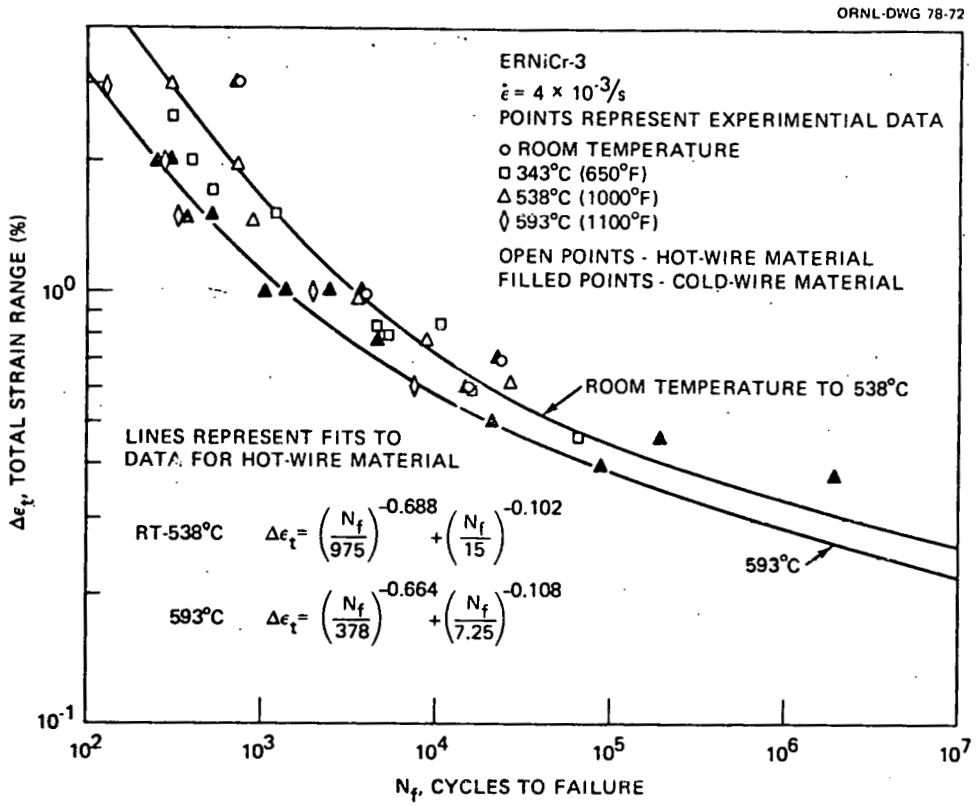

Fig. 8. Relationship Between Strain Range, $\Delta\varepsilon_t$, and Cycles to Failure, N_f, for ERNiCr-3. Experimental fatigue lives are related to predicted fatigue lives.

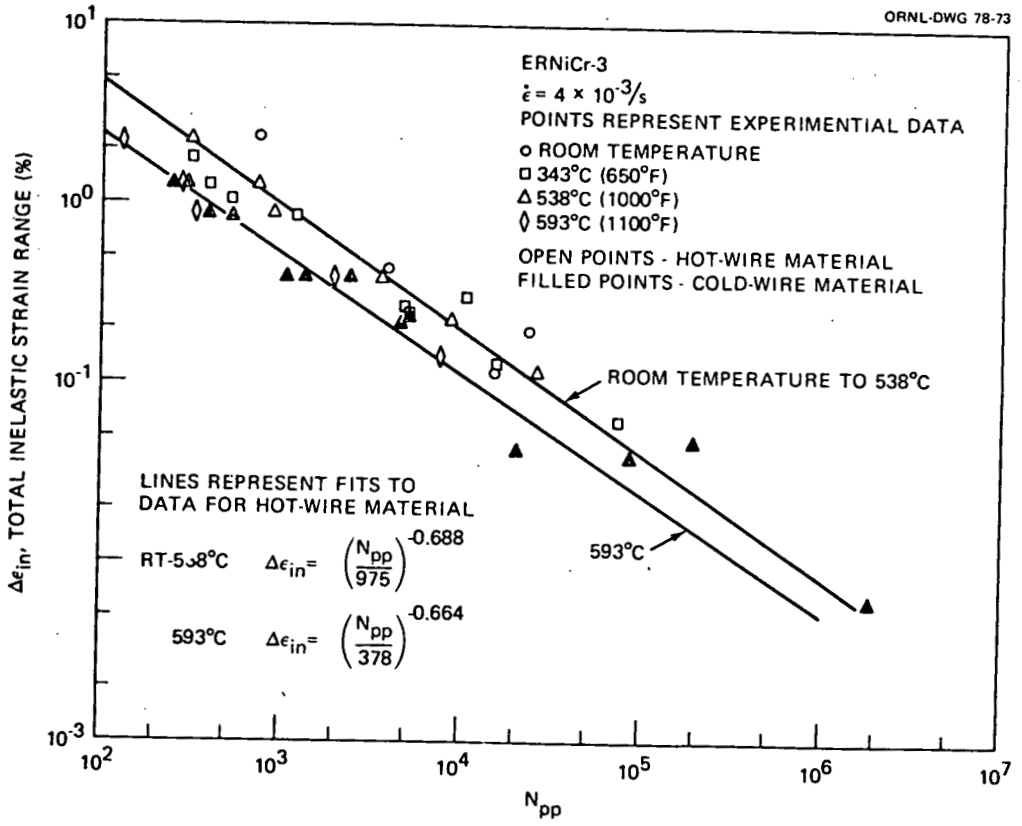

Fig. 9. Relationship Between Plastic Strain Range, $\Delta\varepsilon_p$, and Fatigue Life, N_{pp}, Showing Experimental Data and Predictions.

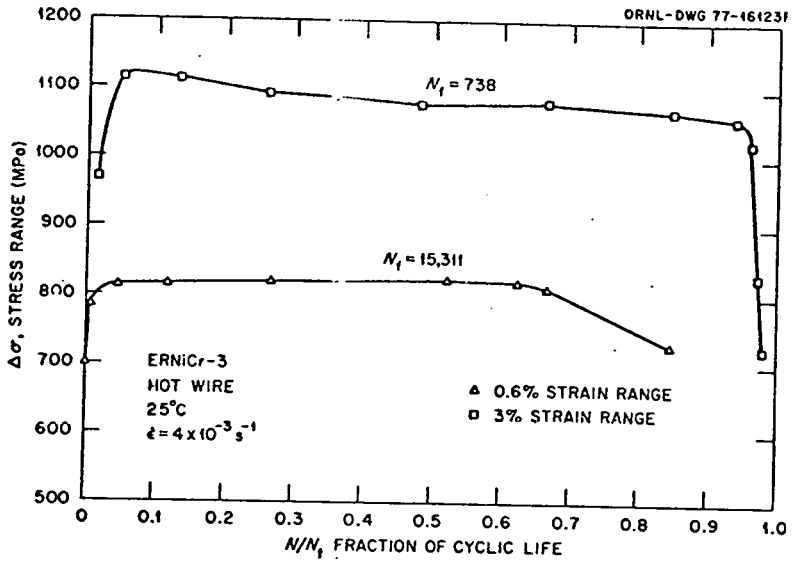

Fig. 10. Measured Stress Range During Cycling of Hot Wire ERNiCr-3 at Room Temperature (25°C) as a Function of Fraction of Cyclic Life.

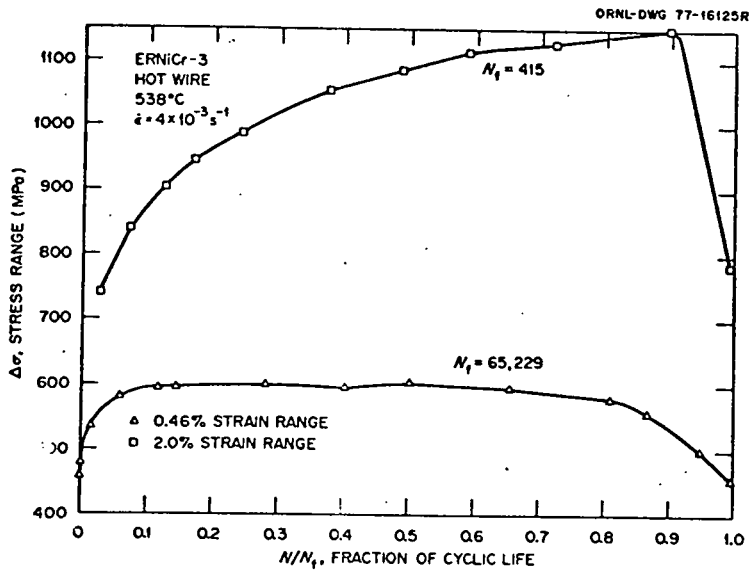

Fig. 11. Measured Stress Range During Cycling of Hot Wire ERNiCr-3 at 538°C as Related to Fraction of Cyclic Life.

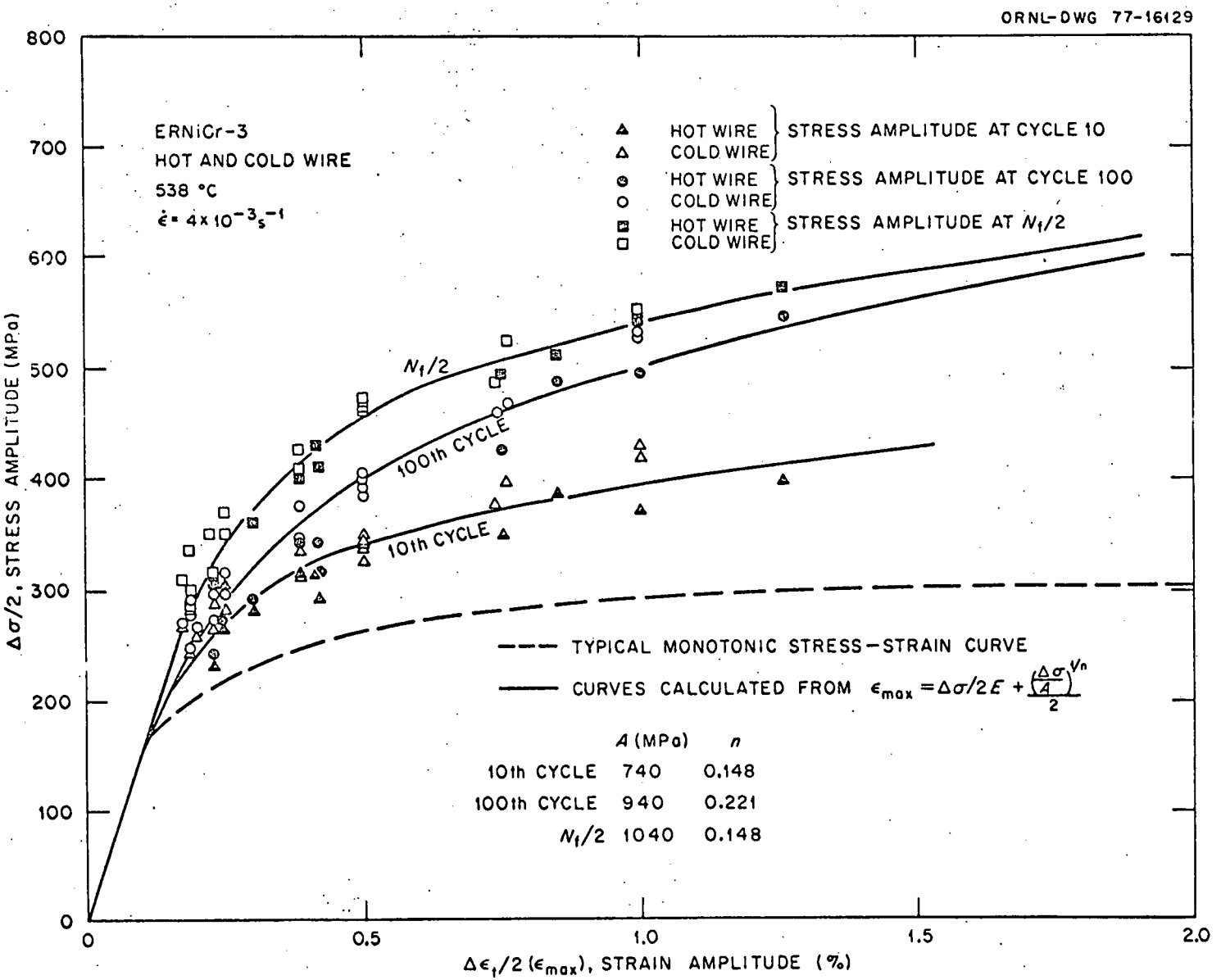

Fig. 12. Cyclic Stress-Strain Curves for ERNiCr-3 as Obtained from Three Cycles of Fatigue Tests. Data and predictions are shown in relation to the monotonic curve.

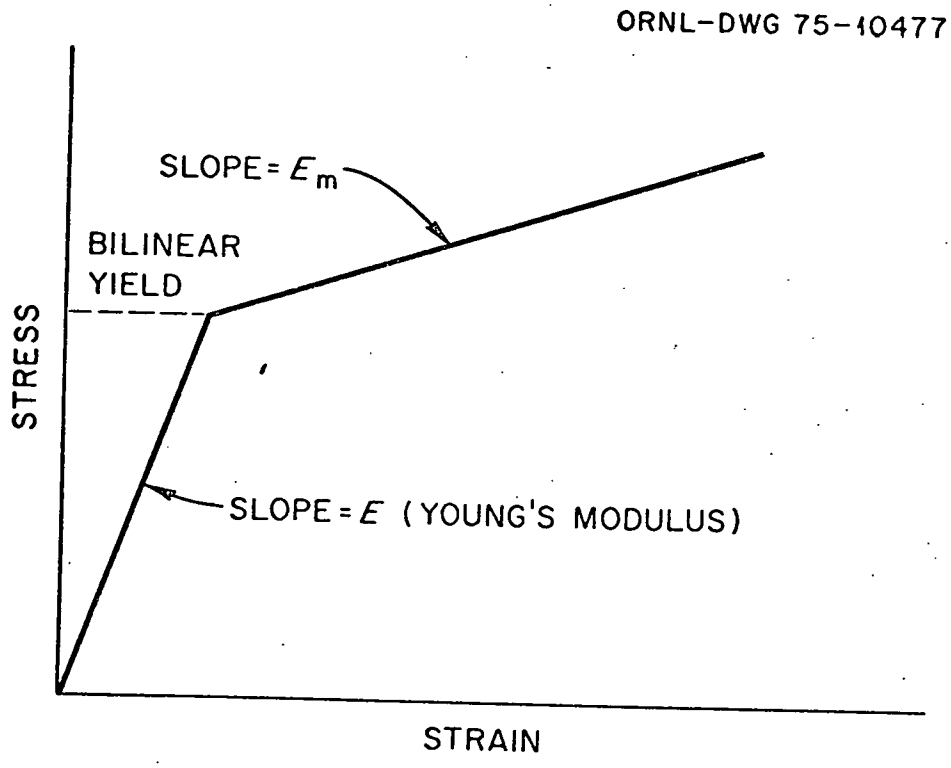

Fig. 13. A Typical Bilinear Stress-Strain Curve.

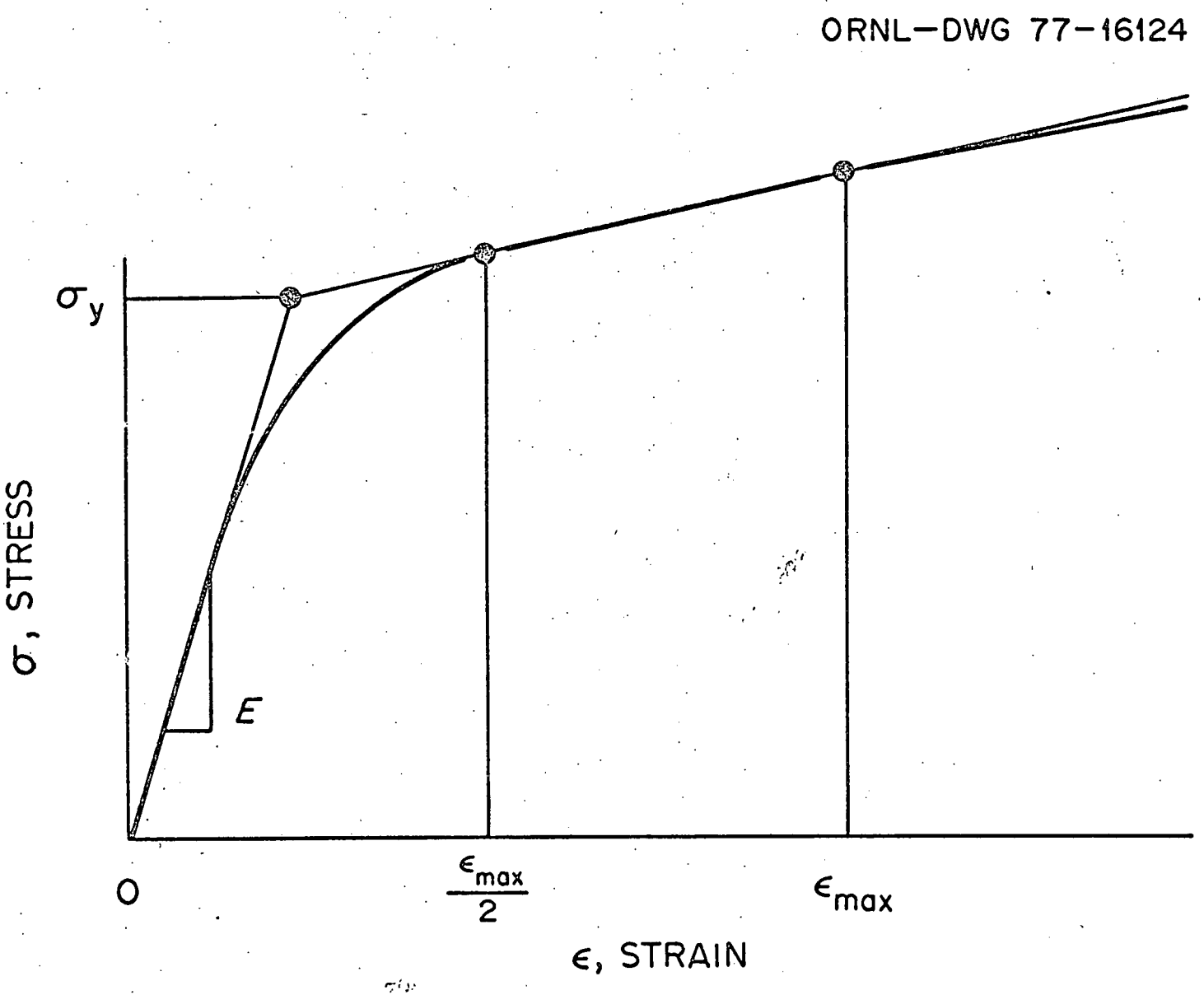

Fig. 14. Construction of a Bilinear Curve from a Monotonic Stress-Strain Curve.

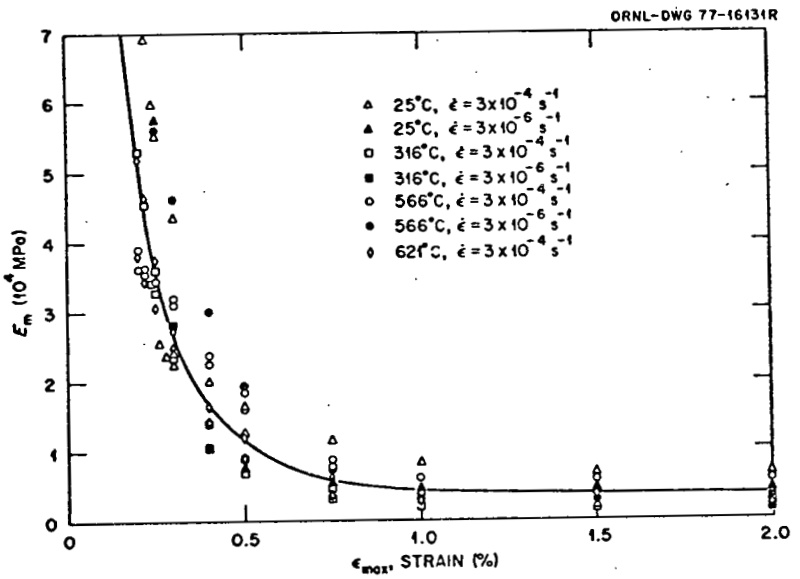

Fig. 15. Data and Mean Curve for E_m as a Function of ϵ_{max} for ERNiCr-3 Obtained from Bilinearization of Tensile Curves.

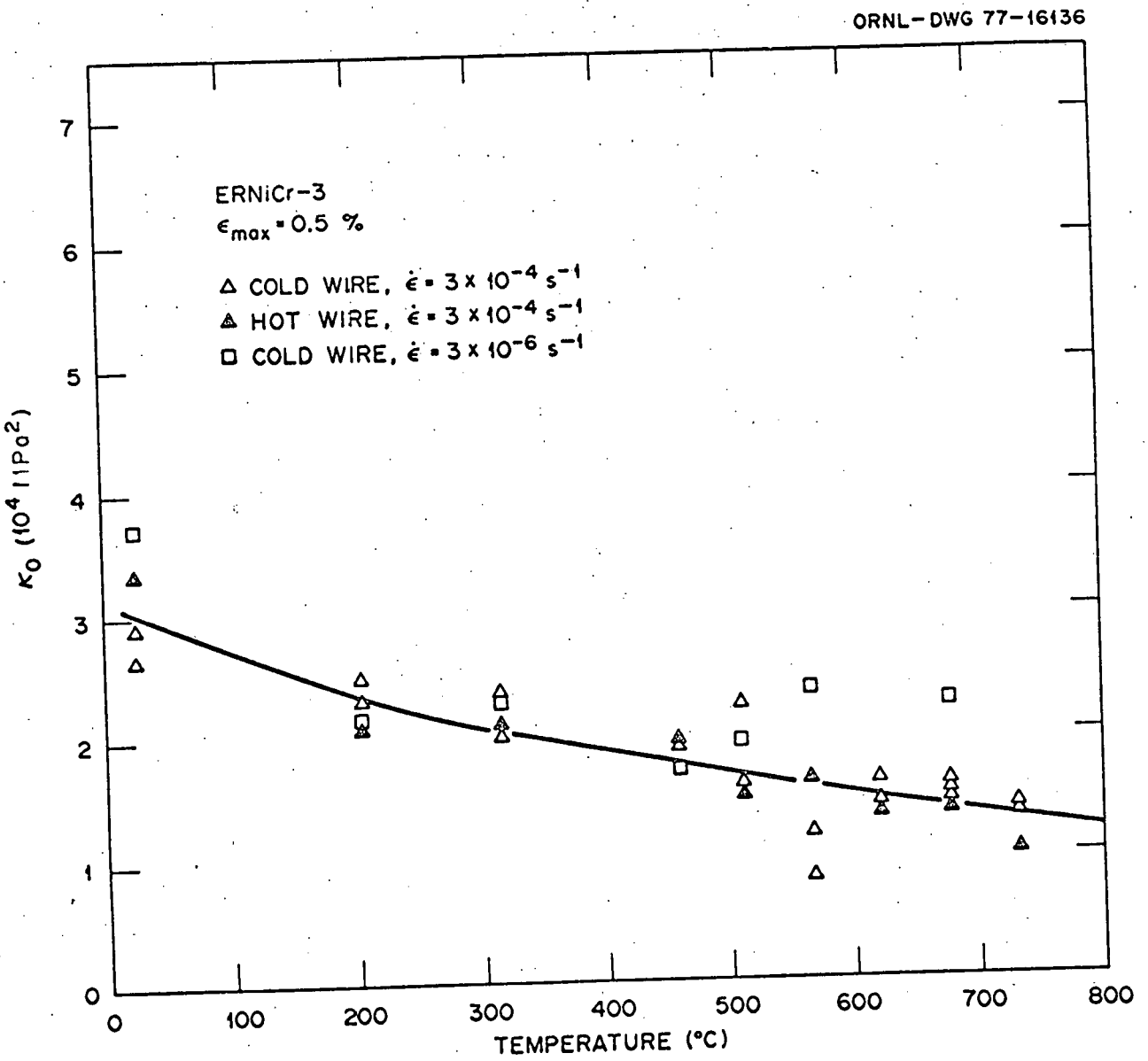

Fig. 16. Variation of K_o with Temperature for ERNiCr-3 at 0.5% Strain.

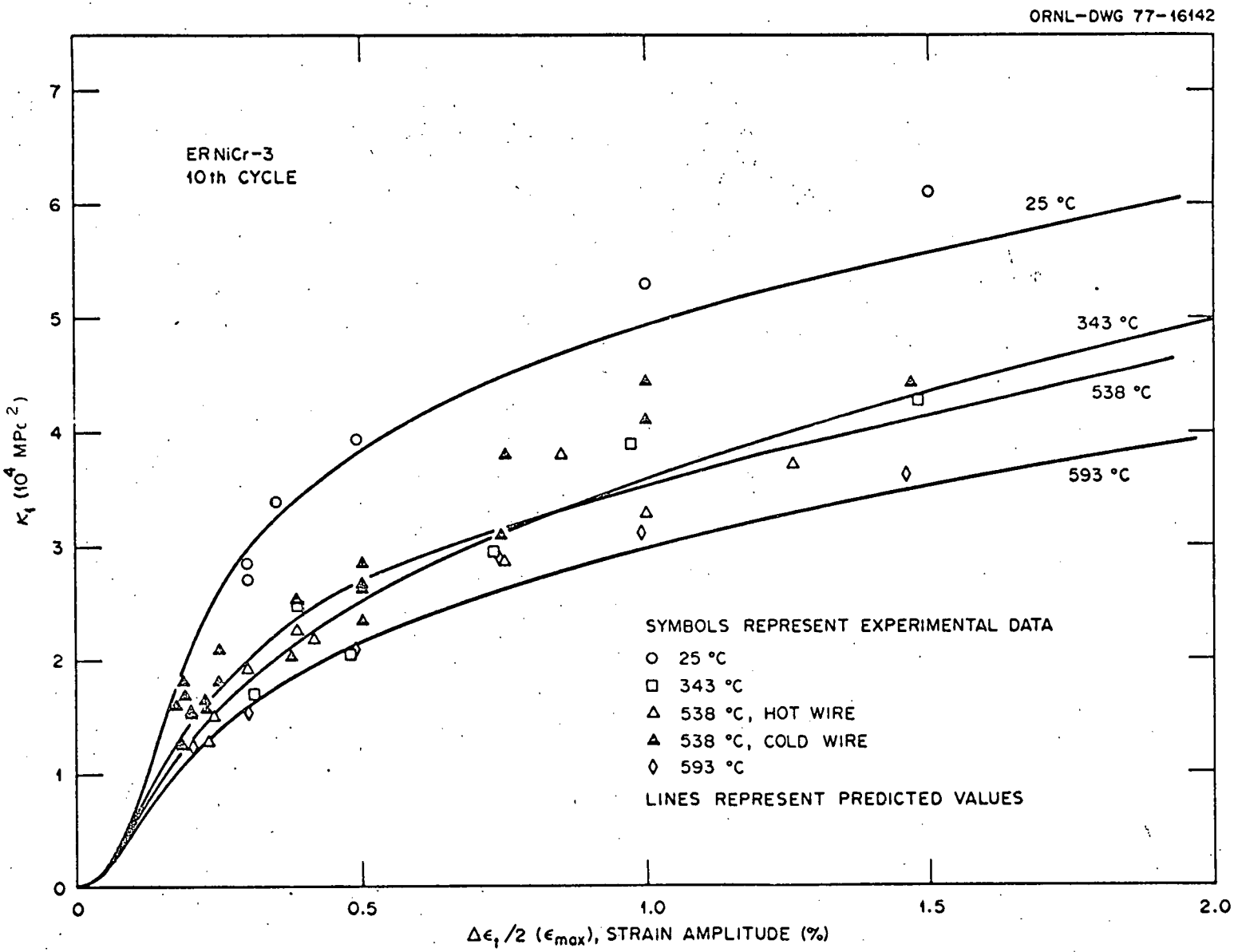

Fig. 17. Relationship Between K and Strain Amplitude, $\Delta\varepsilon_t/2$, for ERNiCr-3 as Calculated from the 10th Cycle of Cyclic Stress-Strain Tests. Predictions of K from the isothermal power law are also shown.

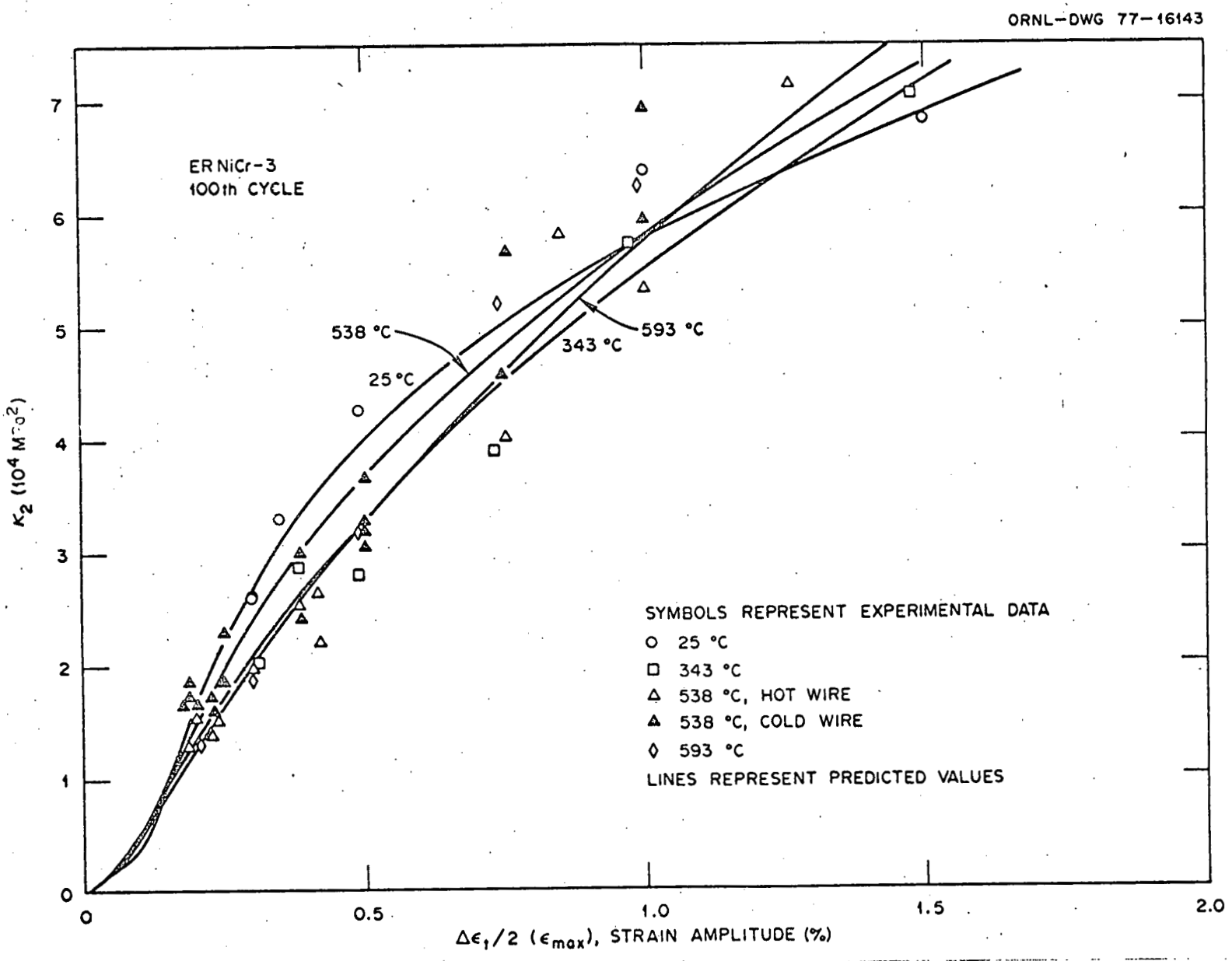

Fig. 18. Relationship Between K and Strain Amplitude, $\Delta\varepsilon_t/2$, for ERNiCr-3 as Calculated from the 100th Cycle of Cyclic Stress-Strain Tests. Predictions of K from the isothermal power law are also shown.

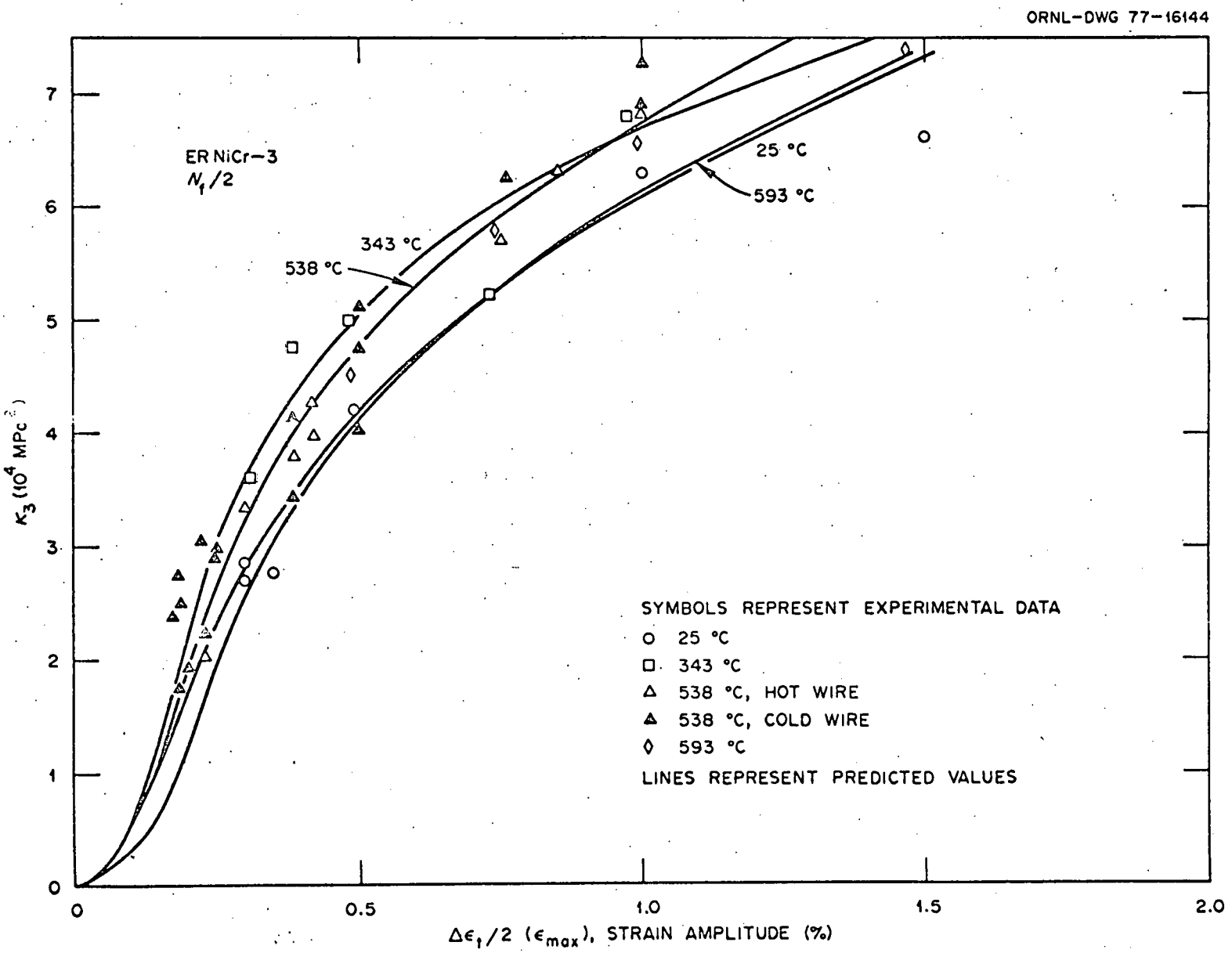

Fig. 19. Relationship Between K and Strain Amplitude, $\Delta\varepsilon_t/2$, for ERNiCr-3 as Calculated at $N_f/2$ of Cyclic Stress-Strain Tests. Predictions of K from the isothermal power law are also shown.

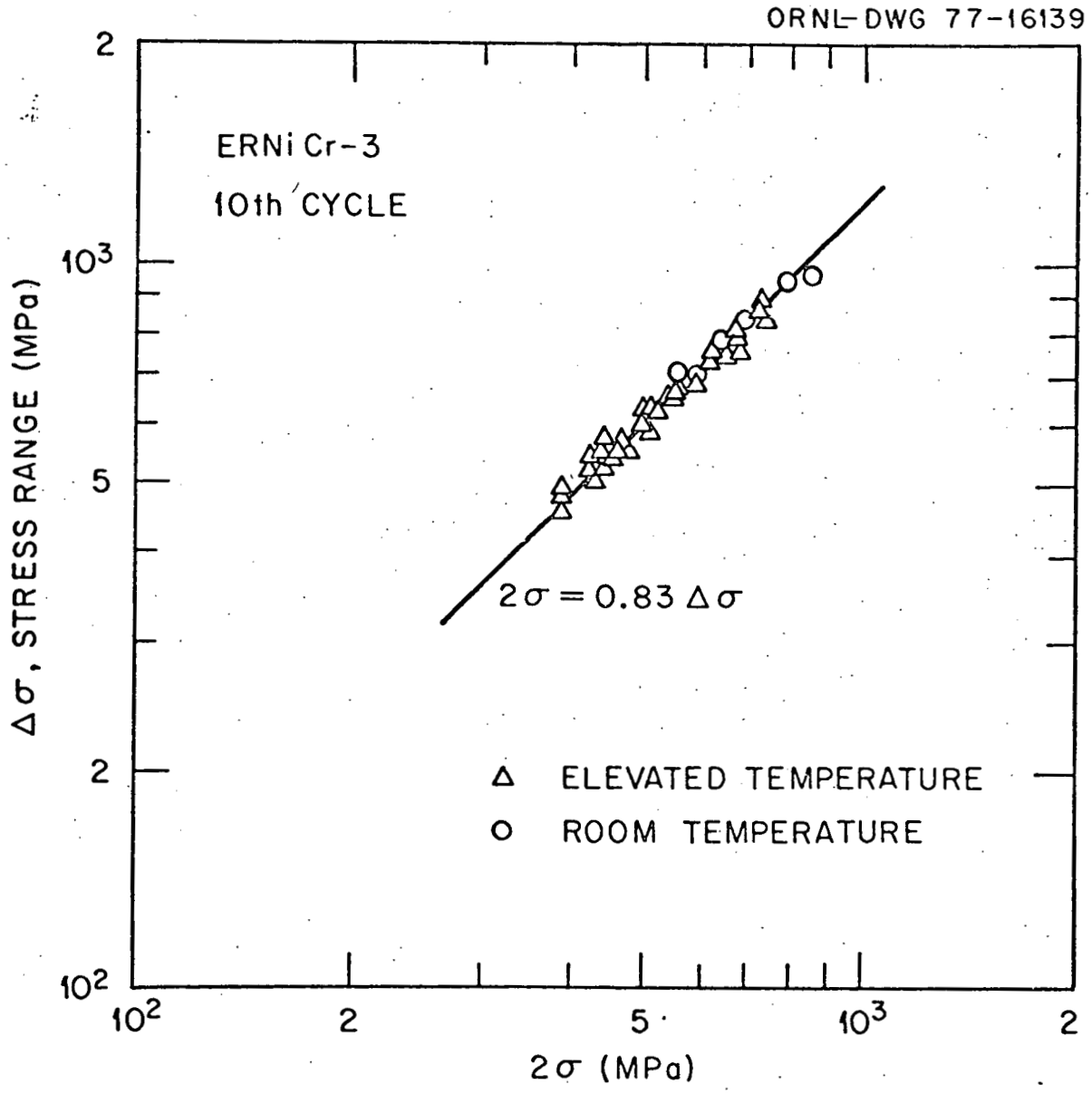

Fig. 20. Experimental Data and Linear Best Fit for $\Delta\sigma$ as a Function of 2σ at the 10th Cycle.

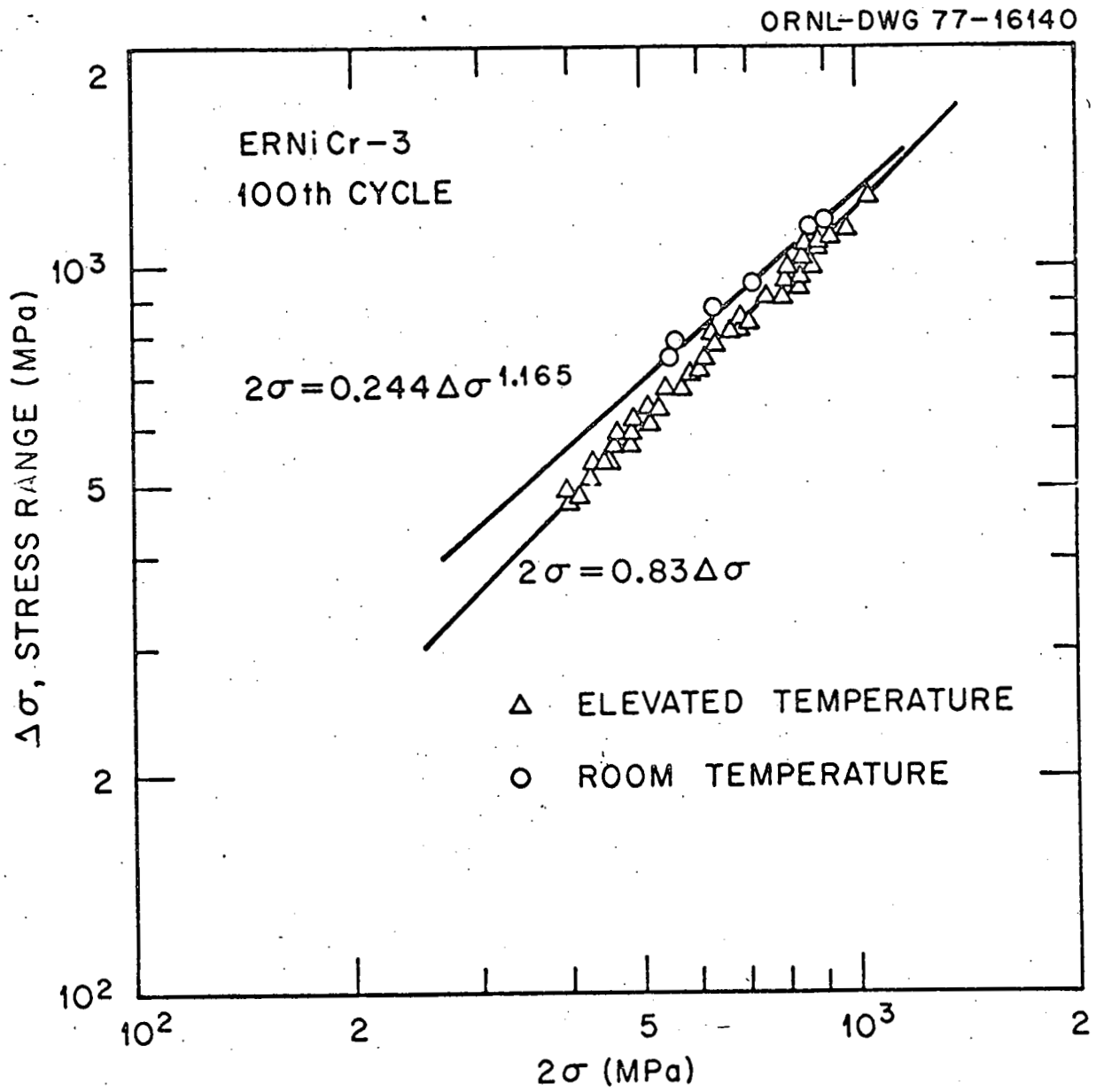

Fig. 21. Experimental Data and Linear Best Fit for $\Delta\sigma$ as a Function of 2σ at the 100th Cycle.

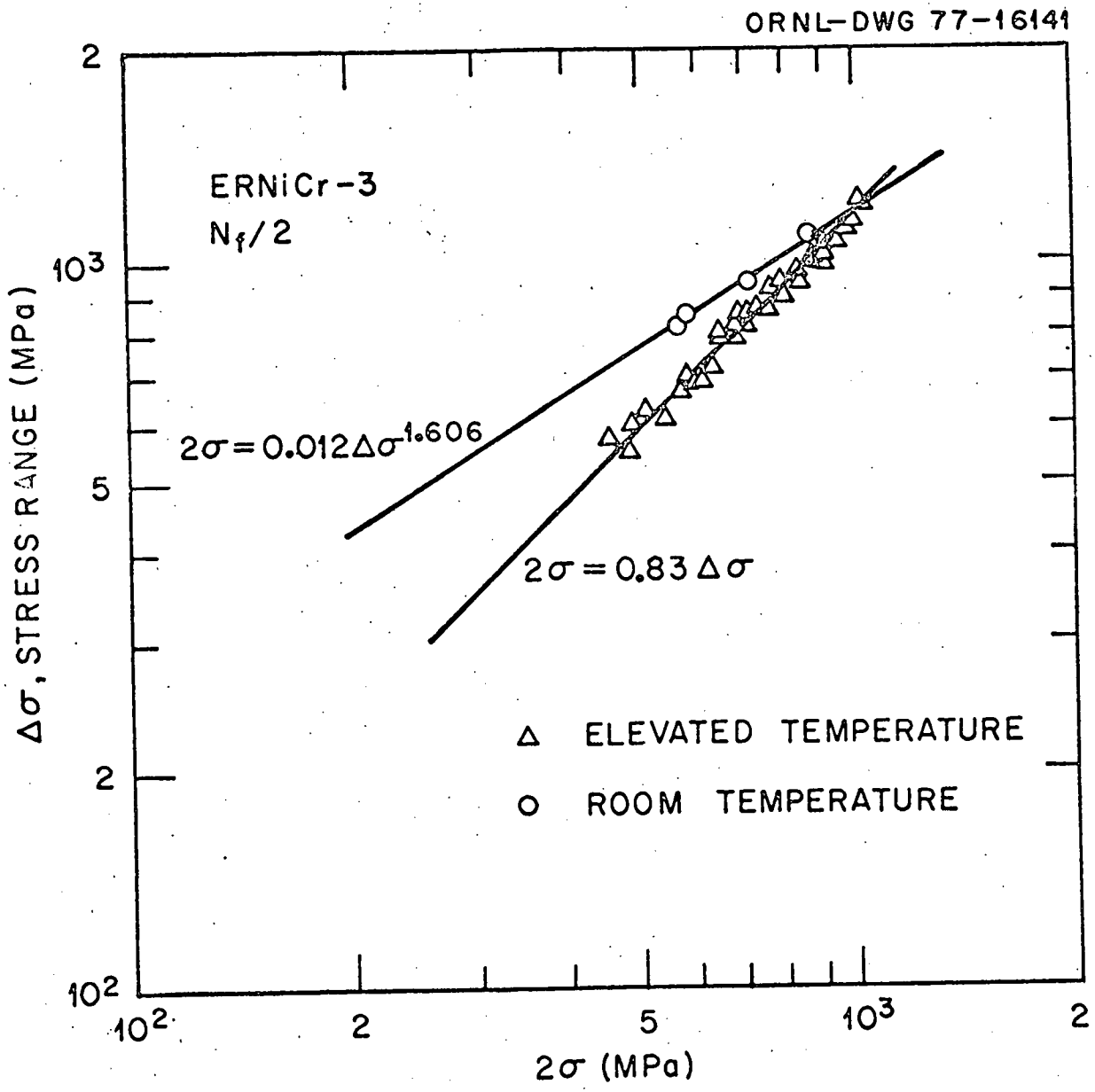

Fig. 22. Experimental Data and Linear Best Fit for $\Delta\sigma$ as a Function of 2σ at $N_f/2$.